# Induced anisotropies in a ferromagnet coupled to a polycrystalline antiferromagnet

Jyotirmoy Saha,[1] Kevin Garello,[2,3,4] B. Viala,[2,3] A. Marty,[1] and N. Vukadinovic[5]
[1]*CEA, INAC/SP2M/NM, 38054 Grenoble, Cedex 9, France*
[2]*CEA, LETI, MINATEC, 38054 Grenoble, France*
[3]*SPINTEC, CEA, CNRS, INPG, CEA/INAC, UJF, 38054 Grenoble, France*
[4]*XLIM, CNRS, 87060 Limoges, France*
[5]*Dassault Aviation, 92552 Saint-Cloud, France*
(Received 22 December 2009; published 22 January 2010)

The effect of thermal activation of a polycrystalline antiferromagnet (AF) coupled to a ferromagnet (FM) on the unidirectional anisotropy responsible for positive shift of the resonant frequency ($f_R$) of the FM is presented. Hysteresis loops and ferromagnetic resonance plots of $Co_{35}Fe_{65}/Ni_{50}Mn_{50}$ are evaluated and matched with those obtained from experiments. The contribution of the AF magnetic structure to $f_R$ is highlighted. An inverse relation between $f_R$ and AF grain size is predicted.

DOI: 10.1103/PhysRevB.81.024417 PACS number(s): 75.30.Gw, 75.50.Ee, 75.60.−d, 76.50.+g

## I. INTRODUCTION

When a ferromagnet (FM) is coupled to a polycrystalline antiferromagnet (AF), the magnetocrystalline anisotropy of the AF induces various forms of anisotropies in the FM mediated by uncompensated spins[1,2] at the AF-FM interface (henceforth, interface). The tuning of these anisotropies has been an important endeavor for industries in the development of spin valve and microwave devices.[3] The two basic yet cardinal experimental outcomes that quantify these anisotropies are: (1) hysteresis loops (HLs) yielding exchange bias ($H_E$) and enhanced coercivity ($H_{EC}$) and (2) ferromagnetic resonance (FMR) plots yielding the resonant frequency ($f_R$). The important distinction between these two classes of experiments is that $H_E$ is a measure of the induced unidirectional anisotropy (henceforth, UA) in the FM as the FM switches between the two magnetic states whereas $f_R$ is a perturbative measure of the UA about the ground state of the system.[4,5] In either case thermal activation of the AF primarily regulates the UA albeit in disparate ways. A strong research focus has been to formulate a canonical connection between these two classes of UA but an overall consensus in this matter is still at large. To achieve this, most (prior) endeavors have estimated $f_R$ utilizing information from experimental HLs and tailoring techniques using the single domain particle (Kittel) approach.[4,6,7] These techniques are system specific and moreover do not present a treatment of the thermal activation of the large AF degrees of freedom. Further progress in this field necessitates a theoretical model that can independently evaluate the FMR profiles and HLs in a multitude of systems based on system (material) attributes. An earlier work reported a model that evaluates HLs and also studied this aspect of AF/FM systems extensively.[8] Utilizing building blocks of this model, in this paper we present a technique to evaluate the FMR response of AF/FM systems. Here, we investigate two metallic systems that are of current technological relevance: (1) $Co_{35}Fe_{65}/Ni_{50}Mn_{50}$ (henceforth CoFe/NiMn) and (2) $Ni_{80}Fe_{20}/Ni_{50}Mn_{50}$ (henceforth Py/NiMn). Experiments are carried out for the CoFe/NiMn system and the model predictions for the Py/NiMn system are compared to existing reports.

## II. EXPERIMENTAL DETAILS AND MATERIAL CHARACTERISTICS

The experimental magnetic bilayer structure consists of: $Si(525\ \mu m)/SiO_2(2\ \mu m)/Ru(5\ nm)/Ni_{50}Mn_{50}(t_{AF}=50\ nm)/Co_{35}Fe_{65}(t_{FM})/Ru(5nm)$ with $t_{FM}=10$ nm, 15 nm, 20 nm and 25 nm; where, $t_{AF}$ ($t_{FM}$) is the AF (FM) thickness. The composite system has an area of $4\times4$ mm$^2$. They are grown by RF-magnetron sputtering on thermally oxidized silicon. The deposition is done at room temperature in the absence of a magnetic field with a base pressure of $9\times10^{-8}$ mbar and an Argon plasma pressure of $2\times10^{-3}$ mbar. Following deposition, the composite system is annealed in vacuum for an hour at 573 K in an applied field of 500 Oe to induce the undirectional anisotropy in the system. The HLs are obtained using a vibrating sample magnetometer (VSM). Post annealing, the $Co_{35}Fe_{65}$ free layer has a saturation magnetization ($M_S$) of $1.87\times10^3$ emu/cc and the easy axis loop yields a coercivity of 17.5 Oe. The complex permeability spectra of the samples are measured from 0.1–10 GHz using a refined single-loop coil technique, based on the model of Bekker *et al.*[9] The small amplitude radio frequency (rf) field is applied perpendicular to the field-cooling direction. The magnetic characteristics of CoFe (Py) used in the model are: $M_S=1.8\times10^3$ emu/cc ($8.6\times10^2$ emu/cc),[8,10] uniaxial magnetocrystalline anisotropy ($K_{FM}$)$=1.57\times10^4$ ergs/cc ($4.3\times10^3$ ergs/cc),[8,10,11] Curie temperature ($T_C$)$=1299$ K (850 K),[8,12] exchange constant ($A_{exchange}$)$=1.75\times10^{-6}$ ergs/cm ($1.0\times10^{-6}$ ergs/cm),[8,10] and damping parameter ($\alpha$)$=0.005$ (0.02).[8,10] The magnetic structure of NiMn incorporates a biaxial in-plane (easy plane) magnetocrystalline anisotropy ($K_{AF}$) of $5\times10^5$ ergs/cc in the (001) plane and an out-of-plane anisotropy of $5.8\times10^6$ ergs/cc and grows with the ⟨111⟩ texturing.[13] The interfacial AF moments are restricted to this (easy) plane due to the absence of an energy scale that can match the out-of-plane anisotropy. The density of lattice sites ($D_{lattice}$) at the interface is $8.64\times10^{14}$ sites/cm$^2$ and the Néel temperature ($T_N$) of NiMn is 1070 K.[13]

## III. THEORETICAL MODEL

In the model the FM layer is treated micromagnetically, a thin sample of FM is discretized into uniformly magnetized

 

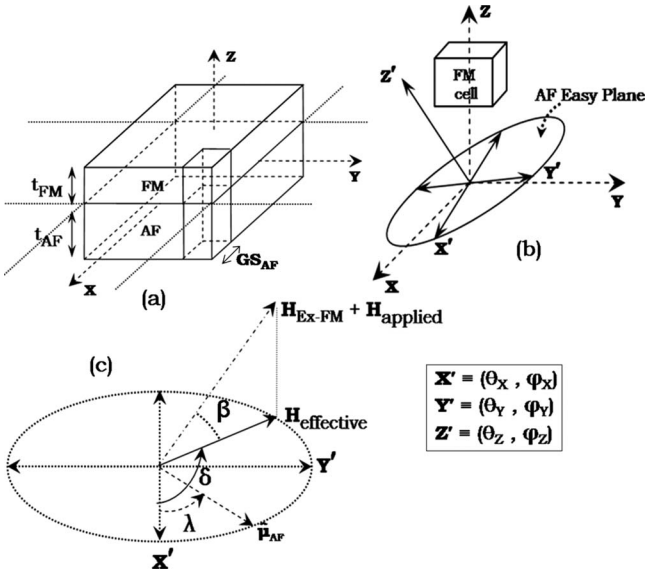


FIG. 1. (a) Discretization of the AF and FM layers; (b) easy plane (001) of an AF grain with respect to its texturing ⟨111⟩, the $\mathbf{X}'$,$\mathbf{Y}'$,$\mathbf{Z}'$ axes are denoted by their spherical angles with respect to the **X**-**Y**-**Z** coordinate system, $\theta_Z$=54.7°; and (c) easy plane of an AF grain. $H_{ex\text{-}FM}$ is the exchange field on an AF grain due to the interaction with the FM cell [Eq. (1)].

rectangular parallelepipeds with a square interface that couples with an AF grain [Fig. 1(a)]. The AF grains are considered noninteracting. The coupling energy[14] between each FM cell and the corresponding AF grain is

$$E_{\text{AF-FM}} = -\,\mathrm{J}_{\text{int}}\tilde{N}\hat{\boldsymbol{\mu}}_{\text{AF}}\cdot\hat{\boldsymbol{\mu}}_{\text{FM}}, \tag{1}$$

where, $J_{\text{int}}=6\sqrt{J_{\text{FM}}J_{\text{AF}}}/(N_{\text{int}}+1)$; $\tilde{N}$ is the net imbalance of the moment direction at the interface due to uncompensated spins; $\hat{\boldsymbol{\mu}}_{\text{AF}}$ is the direction of the net AF moment ($\tilde{N}\boldsymbol{\mu}_{\text{AF}}$) induced at the interface; and $\boldsymbol{\mu}_{\text{FM}}=M_S V_{\text{FM}}\hat{\boldsymbol{\mu}}_{\text{FM}}$, where $V_{\text{FM}}$ is the volume of the FM cell. $J_{\text{FM}}$ and $J_{\text{AF}}$ are estimated in the mean field sense from the knowledge of $T_C$ and $T_N$. $N_{\text{int}}$ is the number of interdiffused interfacial monolayers (chosen to be 1) which corresponds to an AF-FM interface thickness of 4.2 Å.[13] The time evolution of each FM degree of freedom is evaluated by numerically integrating the Landau-Lifshitz-Gilbert equation: $\frac{d\boldsymbol{\mu}_{\text{FM}}}{dt}=-\left(\frac{\gamma}{1+\alpha^2}\right)\boldsymbol{\mu}_{\text{FM}}\times\mathbf{H}-\left(\frac{\alpha\gamma}{1+\alpha^2}\right)\hat{\boldsymbol{\mu}}_{\text{FM}}\times(\boldsymbol{\mu}_{\text{FM}}\times\mathbf{H})$; where $\gamma$ is the gyromagnetic ratio of the free electron and **H** is the net field experienced by a FM cell.[15]

The energy ($E_{\text{AF}}$) of each AF grain of volume $V_{\text{AF}}$ is considered within the framework of a uniform rotation model [Fig. 1(c)]

$$E_{\text{AF}} = 2K_{\text{AF}}V_{\text{AF}}\left[\frac{\sin^2 2\lambda}{8} - \mathrm{h}\cos(\delta-\lambda)\right], \tag{2}$$

where $h\sim\frac{J_{\text{int}}\tilde{N}}{2K_{\text{AF}}V_{\text{AF}}}\cos(\beta)$. The time evolution of $\tilde{N}\boldsymbol{\mu}_{\text{AF}}$ of each AF grain is determined by its ability to switch over energy barriers ($E_{\text{Barrier}}$) to a lower energy state.[8]

The switching occurs when the Néel-Arrhenius condition is satisfied

$$E_{\text{Thermal}} \geq E_{\text{Barrier}} \tag{3}$$

where $E_{\text{Thermal}}=k_B T\ln(2f_O t_{SW})$; where, $k_B$ is the Boltzmann constant, $f_O$(=1 GHz) is the attempt frequency, $t_{SW}$ is the time available for the AF grain to switch and is estimated from typical VSM sweep rates. To incorporate the polycrystalline nature of the AF, $\varphi_Z$, and $\varphi_X$ [Fig. 1(b)] are uniformly distributed in the range $[0,2\pi]$. $\hat{\boldsymbol{\mu}}_{\text{FM}}$ and λ [Fig. 1(c)] are initialized randomly. To set the UA, a field of 1000 Oe along **X** (Fig. 1) is selected and a temperature of 1000 K is chosen. To compute the HL, the applied field is swept along the ±**X** direction. To evaluate the frequency response of the system, the zero-applied-field equilibrium value of the average FM magnetization ($\mathbf{M}_O$) is noted. An impulse[16] along the **Y** direction (Fig. 1) is applied and the system is then allowed to relax back to $\mathbf{M}_O$. As the system relaxes, the quantity $\mathbf{M}_O-\mathbf{M}(t)$ is recorded where $\mathbf{M}(t)$ is the average FM magnetization as a function of time. The discrete Fourier transform of the **Y** component of $\mathbf{M}_O-\mathbf{M}(t)$ yields the real and imaginary (absorption) part of the response of the system. All model calculations are evaluated at $T$=300 K with 64×64 elements. This size yields a system average good enough to be compared to experimental results.[8,14]

## IV. RESULTS AND DISCUSSION

In the CoFe/NiMn system, we estimate the average AF grain size ($GS_{AF}$) in the experimental sample by comparing the experimentally obtained HL to those obtained from model calculations with typical $GS_{AF}$ values[17,18] as observed in metallic systems. For $t_{FM}$=20 nm and $t_{AF}$=50 nm and using $GS_{AF}$=40, 50, and 60 nm in the model calculations the values obtained are: $H_E$=105, 115, and 110 Oe; $H_{EC}$=71, 50, and 25 Oe, respectively; the experimental values are: $H_E$=105 Oe and $H_{EC}$=40 Oe. A good agreement in both $H_E$ and $H_{EC}$ is obtained for $GS_{AF}$=50 nm and this value of $GS_{AF}$ is retained in the evaluation of FMR response for a similar system. The HLs [Figs. 2(a) and 2(b)] and FMR responses [Figs. 2(c)] obtained from the model and experiment for $t_{FM}$=20 and 25 nm are presented. The ability of the model to predict experimental outcomes with this degree of accuracy is a point of merit especially in the light of absence of adjustable parameters. Table I summarizes the results for $t_{FM}$=25, 20, 15, and 10 nm. The model values (for $f_R$) exceed those of the experimental ones by 16% as $t_{FM}$ is decreased to 10 nm. We attribute this to a possible change in the microstructure of the experimental sample, for example: the average AF grain size,[19] effective grain volume of the FM and one-to-one correspondence between AF-FM grains. We repeat the model calculation for $t_{FM}$=10 nm with a bigger grain size of 70 nm. The results restore the numerical agreement of $H_E$ and $f_R$ to a certain extent between experimental and model outcomes. In the Py($t_{FM}$=25 nm)/NiMn($t_{AF}$=50 nm) system the model predicts $f_R$ ranging from 2.9 to 5.3 GHz for a $GS_{AF}$ variation of 70 to 25 nm, respectively. This brackets the experimentally observed value[7] of 3.5 GHz. We now estimate the typical exchange field ($H_{ex\text{-}AF}$) experienced by an FM cell due to its coupling with the AF grain to examine the $t_{FM}$ dependence of $f_R$. Using Eq. (1), we get

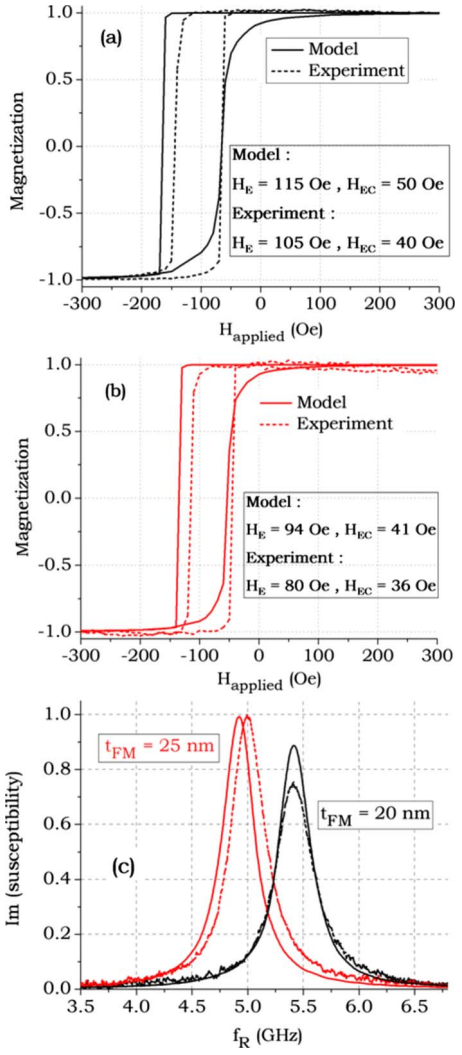


FIG. 2. (Color online) For the CoFe($t_{FM}$)/NiMn($t_{AF}$=50 nm) system: (a) HLs for $t_{FM}$=20 nm; (b) HLs for $t_{FM}$=25 nm; and (c) experimental (dashed lines) and model evaluated (solid lines) FMR response. There exists only one peak in the frequency range 0–10 GHz. The model plots are evaluated with $GS_{AF}$=50 nm.

$$H_{\text{ex-AF}} = \frac{J_{\text{int}}\tilde{N}}{M_S V_{FM}}\langle \hat{\boldsymbol{\mu}}_{AF}\cdot \mathbf{X}\rangle, \tag{4}$$

where $\mathbf{X}$ denotes the UA direction [Figs. 1(b) and 1(c)]. The $\langle\ \rangle$ brackets denote a time average as well as the ensemble average over the polycrystalline degrees of freedom of the AF, $\tilde{N}$ is chosen to be $\sqrt{2N_{\text{total}}/\pi}$ where, $N_{\text{total}}=D_{\text{lattice}}GS_{AF}^2$. The system average UA field ($H_{UA}$) takes the form

$$H_{UA} = H_C + \frac{J_{\text{int}}\sqrt{2D_{\text{lattice}}/\pi}}{M_S GS_{AF} t_{FM}}\langle \hat{\boldsymbol{\mu}}_{AF}\cdot \mathbf{X}\rangle, \tag{5}$$

where $H_C=2K_{FM}/M_S$. The Kittel equation for our film geometry is

$$f_R = (\gamma/2\pi)\sqrt{H_{UA}(H_{UA}+4\pi M_S)}. \tag{6}$$

As $\langle \hat{\boldsymbol{\mu}}_{AF}\cdot \mathbf{X}\rangle$ has no explicit $t_{FM}$ dependence, its ensemble average ($\langle \hat{\boldsymbol{\mu}}_{AF}\cdot \mathbf{X}\rangle_{EAV}$) is adequate to investigate $f_R$ as a function of $t_{FM}$. Figure 3 shows three plots of $f_R$ vs $t_{FM}$ which were obtained: (1) experimentally, (2) from the model, and (3) using Eqs. (5) and (6) with parameter values: $GS_{AF}$ =50 nm, $J_{\text{int}}=18\times10^{-14}$ ergs, $H_C$=17.5 Oe. To estimate $\langle \hat{\boldsymbol{\mu}}_{AF}\cdot \mathbf{X}\rangle_{EAV}$, $\varphi_Z$ is uniformly distributed in the range $[0,2\pi]$, $\varphi_X$ is chosen to be zero (without any loss of generality) and $\lambda$ [Fig. 1(c)] is uniformly distributed in the range $[-\pi/4,\ \pi/4]$. For a quarter million averaging points, $\langle \hat{\boldsymbol{\mu}}_{AF}\cdot \mathbf{X}\rangle_{EAV}$ yields 0.74. Experiments have demonstrated a similar trend.[20,21] The deviation of the single domain particle prediction from the model prediction at low $t_{FM}$ (Fig. 3) is not intuitively straightforward but can be loosely put as: for low $t_{FM}$, $\langle \hat{\boldsymbol{\mu}}_{AF}\cdot \mathbf{X}\rangle_{EAV}$ decreases with the finiteness of $A_{\text{exchange}}$.

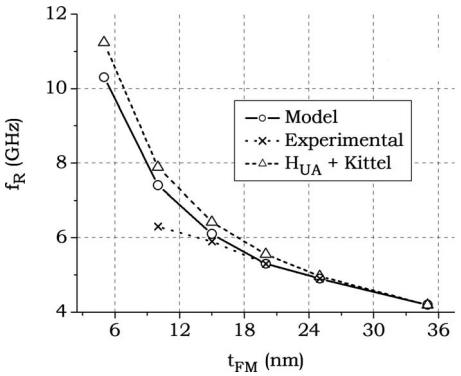


FIG. 3. $f_R$ vs $t_{FM}$ plots for CoFe/NiMn ($t_{AF}$=50 nm) system. The theoretical plots are evaluated with $GS_{AF}$=50 nm. Lines are a guide to the eye.

The model evaluated $f_R$ vs $t_{AF}$ plot is shown in Fig. 4(a). We will discuss below the case: $GS_{AF}$=50 nm as a similar discussion holds for $GS_{AF}$=30 nm. A decrease in $t_{AF}$ below 45 nm increases the population of the AF grains satisfying the condition: $K_{AF}V_{AF} \ll 4J_{\text{int}}\tilde{N}$. Such grains are devoid of energy barriers [Eq. (2)] thereby turning superparamagnetic. These grains readily trail (align with) the FM moments responding to the rf field. Their inability to consolidate the UA direction results in the reduction in $H_{UA}$. An increase in $t_{AF}$ from 45 to 75 nm stabilizes the AF grains and pins them in their field-cooling configuration resulting in an increase in $H_{UA}$. This increase reaches a maximum value denoting an optimum number of AF grains consolidating the UA direc-

TABLE I. Exchange bias ($H_E$), enhanced coercivity ($H_{EC}$), and resonance frequency ($f_R$) obtained from experiments (exp.) and model calculations for CoFe($t_{FM}$)/NiMn($t_{AF}$=50 nm). Model calculations are done with $GS_{AF}$=50 nm. ( * denotes the model calculations with $GS_{AF}$=70 nm.)

| $t_{FM}$ (nm) | $H_E$ (model) (Oe) | $H_E$ (exp.) (Oe) | $H_{EC}$ (model) (Oe) | $H_{EC}$ (exp.) (Oe) | $f_R$ (model) (GHz) | $f_R$ (exp.) (GHz) |
|---|---|---|---|---|---|---|
| 25 | 94 | 80 | 41 | 36 | 4.9 | 5.0 |
| 20 | 115 | 105 | 50 | 40 | 5.4 | 5.4 |
| 15 | 148 | 119 | 59 | 39 | 6.2 | 5.9 |
| 10 | 226 190* | 140 | 78 23* | 56 | 7.4 6.0* | 6.4 |

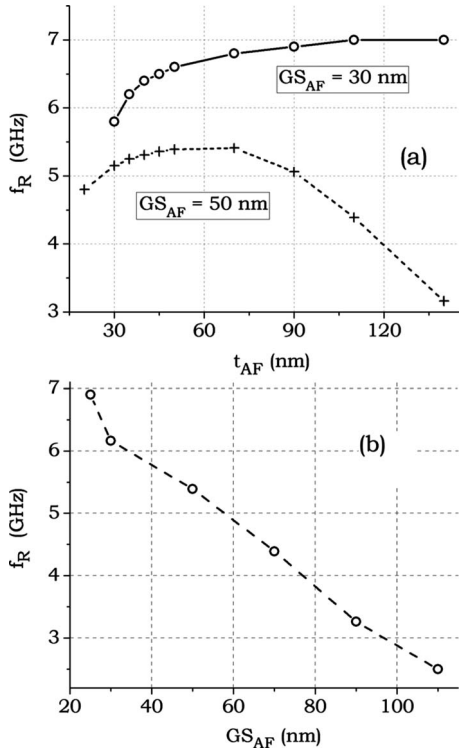


FIG. 4. Model evaluated: (a) $f_R$ vs $t_{AF}$ for CoFe ($t_{FM}$=20 nm)/NiMn with $GS_{AF}$=30 nm (open circle symbols), 50 nm [(+) symbols] and (b) $f_R$ vs $GS_{AF}$ for CoFe ($t_{FM}$=20 nm)/NiMn($t_{AF}$=50nm). Lines are a guide to the eye.

tion. Beyond this maximum ($t_{AF}>75$ nm), a further increase in $t_{AF}$ results in an additional number of AF grains attaining thermal stability but the net angular dispersion in $\hat{\boldsymbol{\mu}}_{AF}$ reduce $H_{UA}$. This reduction in $H_{UA}$ is mainly dictated by the magnetic structure of the AF $\langle \hat{\boldsymbol{\mu}}_{AF} \cdot \mathbf{X} \rangle_{EAV}$. A similar trend of $f_R$ vs $t_{AF}$ has also been experimentally observed.[4,22] Next we discuss the $GS_{AF}$ dependence of $f_R$ [Fig. 4(b)]. An increase in $GS_{AF}$ enhances the locking of the AF grains along the UA direction [Eq. (2)] simultaneously decreasing the UA field [Eq. (5)]. The net effect of these two conflicting contributions is a monotonic decrease in $f_R$ as a function of $GS_{AF}$ [Fig. 4(b)]. This implies that $(J_{int}\sqrt{2D_{lattice}}/\pi/M_S GS_{AF} t_{FM})$ has a dominant contribution over $\langle \hat{\boldsymbol{\mu}}_{AF} \cdot \mathbf{X} \rangle$ in the case of FMR measurements. The nontrivial behaviors of $f_R$ vs $t_{AF}$ and $f_R$ vs $GS_{AF}$ attributable to the thermal activation of the large AF degree of freedom have not been the natural outcome of any previous theoretical work. To estimate the (theoretical) maximum $f_R$ of any particular system from HLs, we (model) compute HLs at $T$=0 K and measure the field ($H_{SW}$) at which the FM magnetization reverses starting from the field-cooled state. For the CoFe($t_{FM}$=20 nm)/NiMn($t_{AF}$=50 nm) system with $GS_{AF}$=50 nm, $H_{SW}$ is 155 Oe which corresponds to a $f_R$ value of 5.3 GHz using $H_{UA}=H_{SW}$ in Eq. (6). This fits well with the values obtained from both the model and the experiment [Fig. 4(a)].

## V. CONCLUSIONS

We have established the tunability of $f_R$ by altering thermal stability of the AF (dictated by $t_{AF}$ and $GS_{AF}$) in an AF/FM system. As the UAs measured by $H_E$ and $f_R$ have different physical origin, a general formula may not be achievable to predict $f_R$ based on information from experimental HLs for a wide range of either $t_{AF}$ or $GS_{AF}$ or temperature. Nevertheless, the maximum attainable $f_R$ in such a system can be estimated from a (experimental) HL evaluated at a temperature (low enough) such that the coercivity of the system is mainly due to the magnetocrystalline anisotropy of the FM.

## ACKNOWLEDGMENTS

This work is supported by the French National Research Agency ANR—INSTITUTS CARNOT. The support of J. C. Toussaint and L. Buda-Prejbeanu in this project is acknowledged.

[1] H. Ohldag, A. Scholl, F. Nolting, E. Arenholz, S. Maat, A. T. Young, M. Carey, and J. Stöhr, Phys. Rev. Lett. **91**, 017203 (2003).
[2] I. N. Krivorotov, C. Leighton, J. Nogués, I. K. Schuller, and E. D. Dahlberg, Phys. Rev. B **68**, 054430 (2003).
[3] B. Viala, G. Visentin, and P. Gaud, IEEE Trans. Magn. **40**, 1996 (2004).
[4] J. McCord, R. Mattheis, and D. Elefant, Phys. Rev. B **70**, 094420 (2004).
[5] R. D. McMichael, M. D. Stiles, P. J. Chen, and W. F. Egelhoff, Jr., Phys. Rev. B **58**, 8605 (1998).
[6] Bijoy K. Kuanr, R. E. Camley, and Z. Celinski, J. Appl. Phys. **93**, 7723 (2003).
[7] D. Spenato, J. Ben Youssef, and H. Le Gall, J. Magn. Magn. Mater. **240**, 254 (2002).
[8] J. Saha and R. H. Victora, Phys. Rev. B **73**, 104433 (2006).
[9] V. Bekker, K. Seemann, and H. Leiste, J. Magn. Magn. Mater. **270**, 327 (2004).
[10] J. O. Rantschler, C. Alexander, Jr., and H.-S. Jung, J. Magn. Magn. Mater. **286**, 262 (2005).
[11] R. H. Yu, S. Basu, L. Ren, Y. Zhang, Azar Parvizi-Majidi, K. M. Unruh, and John Q. Xiao, IEEE Trans. Magn. **36**, 3388 (2000).
[12] T. Fukuda, M. Yuge, T. Terai, and T. Kakeshita, J. Phys.: Conf. Ser. **51**, 307 (2006).
[13] J. S. Kasper and J. S. Kouvel, J. Phys. Chem. Solids **11**, 231 (1959).
[14] J. Saha, J. S. Parker, Bruce T. Bolon, A. Abin-Fuentes, C. Leighton, and R. H. Victora, J. Appl. Phys. **102**, 073901 (2007).
[15] **H** includes the applied field, the demagnetizing field, the exchange field due to $A_{exchange}$, the FM MCA field and the exchange field from the corresponding AF grain as outlined in Ref. 8.
[16] The impulse is chosen such that the system response is linear.
[17] A. Paul, D. E. Bürgler, and P. Grünberg, J. Magn. Magn. Mater.

**286**, 216 (2005).
[18] M. Pakala, Y. Huai, G. Anderson, and L. Miloslavsky, J. Appl. Phys. **87**, 6653 (2000).
[19] Bruce T. Bolon, M. A. Haugen, A. Abin-Fuentes, J. Deneen, C. B. Carter, and C. Leighton, J. Magn. Magn. Mater. **309**, 54 (2007).
[20] O. Acher, S. Queste, K.-U. Barholz, and R. Mattheis, J. Appl. Phys. **93**, 6668 (2003).
[21] Y. Lamy and B. Viala, IEEE Trans. Magn. **42**, 3332 (2006).
[22] S. Queste, S. Dubourg, O. Acher, J.-C. Soret, K.-U. Barholz, and R. Mattheis, J. Magn. Magn. Mater. **288**, 60 (2005).